Surrey *et al. Adv Struct Chem Imag (2016) 2:7*
DOI 10.1186/s40679-016-0022-1

Advanced Structural and Chemical Imaging

RESEARCH Open Access

Electron beam induced dehydrogenation of MgH_2 studied by VEELS

Alexander Surrey[1,2*], Ludwig Schultz[1] and Bernd Rellinghaus[1]

Abstract

Nanosized or nanoconfined hydrides are promising materials for solid-state hydrogen storage. Most of these hydrides, however, degrade fast during the structural characterization utilizing transmission electron microscopy (TEM) upon the irradiation with the imaging electron beam due to radiolysis. We use ball-milled MgH_2 as a reference material for in-situ TEM experiments under low-dose conditions to study and quantitatively understand the electron beam-induced dehydrogenation. For this, valence electron energy loss spectroscopy (VEELS) measurements are conducted in a monochromated FEI Titan^3 80–300 microscope. From observing the plasmonic absorptions it is found that MgH_2 successively converts into Mg upon electron irradiation. The temporal evolution of the spectra is analyzed quantitatively to determine the thickness-dependent, characteristic electron doses for electron energies of both 80 and 300 keV. The measured electron doses can be quantitatively explained by the inelastic scattering of the incident high-energy electrons by the MgH_2 plasmon. The obtained insights are also relevant for the TEM characterization of other hydrides.

Keywords: VEELS, Magnesium hydride, Low dose, Radiolysis, In-situ TEM

Background

Hydrogen is a promising clean energy carrier that has the potential of replacing fossil fuels in a future sustainable economy. However, hydrogen storage in a safe and efficient way remains a challenge. Magnesium hydride, MgH_2, is a promising and well-studied material, because of its high reversible hydrogen storage capacity of 7.6 wt% and its low cost. However, the unfavorable high thermodynamic stability and poor reaction kinetics still limit the application of MgH_2 for hydrogen storage today. Ergo hydrogen desorbs only at temperatures above 300 °C [1], which is impracticable for on-board vehicular applications [2].

High-energy ball milling has been widely used to prepare nanostructured $Mg(H_2)$ based materials with grain sizes in the nanometer regime, which resulted in significantly improved kinetics [1, 3–8]. However, the stabilization of small grain sizes upon cycling and potential thermodynamic improvements could not be achieved with this technique. A further reduction of the MgH_2 particle sizes down to 1 nm is needed for substantial thermodynamic destabilization due to a size effect as predicted by theoretical studies [9, 10]. In the past decade much effort has been devoted to the development of new preparation techniques to produce nanoconfined $Mg(H_2)$ [11–14], which resulted in improved kinetics and in addition to it in the thermodynamic destabilization of MgH_2 [15–19] with decomposition temperatures as low as 50 °C [19].

In all these studies TEM is a vital tool for the structural characterization; however, MgH_2 degrades fast upon the irradiation with the imaging electron beam due to radiolysis [20]. This considerably hinders studying the hydride phase with high spatial resolution, unless a cryogenically cooled liquid nitrogen sample holder is used, which again limits the spatial resolution. The electron-beam-induced dehydrogenation was monitored in-situ by electron diffraction to identify the crystallographic orientation relation between MgH_2 and Mg [21, 22]. This dehydrogenation was further observed in-situ by valence electron energy loss spectroscopy (VEELS) [8, 12, 21], where both phases can be identified by their distinct plasmon

*Correspondence: a.surrey@ifw-dresden.de
[1] IFW Dresden, Institute for Metallic Materials, 01171, 270116 Dresden, Germany
Full list of author information is available at the end of the article

energies [23]. However, little is known about the mechanism governing the rate of the electron-beam-induced dehydrogenation and a quantitative description of this effect is lacking.

Danaie et al. provided a fairly consistent phenomenology for the thermally induced dehydrogenation of MgH_2 based on their energy-filtered TEM (EFTEM) observations of ball-milled MgH_2, which was stabilized in the TEM using a cryogenic sample holder cooled to 90 K [8]. They could rule out a model which assumes that the desorption starts at the surface, forms a growing metal shell and a shrinking hydride core. Instead, the heterogeneous nucleation of the Mg phase is difficult and proceeds only on exposed surfaces and on high-energy defects. Once a nucleus is formed, the metallic phase grows fast, because hydrogen diffusion is fast along grain boundaries. This leads to a grain-by-grain dehydrogenation. The reaction is kinetically limited by solid-state diffusion of ions or atoms towards or away from the reaction front. However, as the authors also pointed out, this applies only to the elevated-temperature-driven dehydrogenation, whereas for the electron-beam-induced dehydrogenation at room temperature the process is different.

In the present study, we provide a detailed quantitative analysis of the electron-beam-induced dehydrogenation of MgH_2 by VEELS under low-dose conditions. A description of this phenomenon consistent with previous studies is given. The influences of incident electron energy, electron current density and specimen thickness are explained quantitatively.

Methods

Sample preperation

Ball milling of the MgH_2 powder (Goldschmidt) was performed under argon atmosphere in a Retsch PM400 planetary ball mill using hardened steel balls and vials. The powder was milled for 80 h at a ball-to-powder mass ratio of 10:1 at a milling intensity of 200 revolutions per minute. All sample handling was carried out in a glove box under purified argon atmosphere (oxygen and water levels less than 1 ppm). The MgH_2 powder was distributed on a TEM copper grid supported with a thin and holey amorphous carbon film. The TEM grid was placed in a TEM vacuum transfer holder inside the glove box, where the specimen tip was retracted in the barrel of the holder. The holder was opened only during the loading cycle into the TEM under vacuum.

Monochromated VEELS

For acquiring the VEEL spectra a FEI Titan^3 80–300 equipped with a monochromator was used in TEM mode. The full width at half maximum of the monochromated zero loss beam is 0.26 and 0.44 eV at accelerating voltages of 80 and 300 kV, respectively. The continuous acquisition of VEEL spectra was realized by a self-written script in Gatan DigitalMicrograph with an exposure time of 0.5 s, a CCD readout area of 512 × 2048 pixels and a pixel binning of 2. With this, a time resolution of 1.5 s per spectrum could be achieved. The 5-mm GIF entrance aperture was used to collect all elastically and inelastically scattered electrons up to a collection angle of 17.6 mrad. In order to avoid the illumination of the specimen prior to the acquisition of the VEELS series, a small round electron beam with a diameter of about 0.5–1 μm was formed. A typical series of VEEL spectra contained about 150 single spectra. The spectra were corrected for energy drift, and plural scattering was removed by deconvolution using the Fourier-log method implemented in the Gatan Digital Micrograph software. The zero loss beam measured in vacuum was used for the de- and reconvolution. The relative thickness of the specimen was calculated for every spectrum using the log-ratio method implemented in Gatan Digital Micrograph according to the relation $d/\lambda = \ln(I_{\mathrm{tot}}/I_0)$, where d is the thickness of the specimen, λ the mean free path of the electrons, I_{tot} is the total intensity of the incident electron beam and I_0 is the intensity of the transmitted zero loss beam [24]. The current density in the area from where the VEEL spectra were acquired was measured using the CCD camera of the energy filter system in TEM mode under identical imaging conditions as during the acquisition of the VEELS series. The conversion factors of the CCD camera are 0.326 and 0.112 electrons per counts at 300 and 80 kV, respectively.

The spectra were quantitatively analyzed in the low-loss region, i.e. energy loss ≤50 eV, by fitting a sum of two Lorentz functions

$$S(E) = L_1(E) + L_2(E) + O \tag{1}$$

with

$$L_i(E) = \frac{2A_i}{\pi}\frac{w_i}{4(E-E_i)^2 + w_i^2}, \quad (i = 1, 2) \tag{2}$$

to the deconvoluted spectra. Here, A_i are the areas of the Lorentz function for the Mg or MgH_2 plasmon with the plasmon energies E_i and the width w_i, respectively. The width and plasmon energy for the MgH_2 and the Mg plasmon are determined by fitting a single Lorentz function to the first and last spectrum of each series, respectively, where only the hydride or metallic phase is present in the specimen. These values were kept fixed for analyzing the whole series and only the areas A_i (and the offset O, which is almost constant) are fitted to the spectra.

Results

X-ray diffraction analysis and Rietveld refinement using the software MAUD [25] reveal that the ball-milled MgH_2 is mainly composed of the tetragonal α-MgH_2 phase with 66 wt% and crystallite sizes in the range of 10 nm. Furthermore, it contains the orthorhombic, high-pressure γ-MgH_2 phase with 33 wt% and crystallites in the range of 70 nm. The X-ray diffraction pattern can be found in Additional file 1: Figure S1. A typical nanocrystalline MgH_2 particle studied by VEELS is shown in Fig. 1. It is located at the edge of the holey carbon substrate. Such agglomerations of MgH_2 nanocrystals are typically 100–600 nm in diameter. Due to the impact of the electron beam the shown particle is already fully dehydrogenated. It is not possible to acquire a TEM bright field image of the ball-milled MgH_2 in the hydrogenated phase with the CCD camera even at low magnifications, since the electron dose, that is needed for an acquisition with the CCD with a decent signal-to-noise ratio, already causes massive dehydrogenation. The red, 36 × 36 nm^2 large square in Fig. 1 depicts the area of the specimens, from where the VEEL spectra are acquired with the CCD camera of the energy filter system under low-dose conditions.

Figure 2 shows as examples three VEEL spectra of a typical dehydrogenation of a nanocrystalline MgH_2 particle irradiated with 300 keV electrons of a current density of 818 $e^-/nm^2/s$. The initial broad MgH_2 plasmon at 14.1 eV that is clearly visible in Fig. 2a starts to decrease, as soon as the specimen is exposed to the electron beam. At an intermediate state, the additional sharp plasmon peak of metallic Mg at 10.1 eV is observable in Fig. 2b. After approximately 3 min, most of the hydrogen has left the specimen, and the spectrum in Fig. 2c is dominated by the Mg plasmon. The amount of each phase present in the specimen is reflected by the areas under the respective plasmon peaks. There is no overlaid carbon plasmon, which would be centered around 20–34 eV, since the VEEL spectra of the MgH_2 particle are acquired from an area above a hole of the carbon substrate. Due to the use of the vacuum transfer holder the oxidation of the specimen can be minimized, which can be seen from the lack of any MgO volume plasmon at ca. 23 eV [8]. The only signals in the spectra originate from the single inelastic scattering with the Mg and MgH_2 volume plasmons, because the spectra are corrected for plural scattering by deconvolution with the Fourier-log method which also removes the zero-loss beam. The sum of two Lorentz functions describing the two plasmons can be fitted to the spectra very accurately. The adjusted coefficients of determination, $\bar{R}^2$, describing the goodness of the fits are generally around 0.95 or better. Only for the intermediate states, where both plasmons are present, the goodness of fit is occasionally worse with $\bar{R}^2 = 0.8 - 0.9$. This

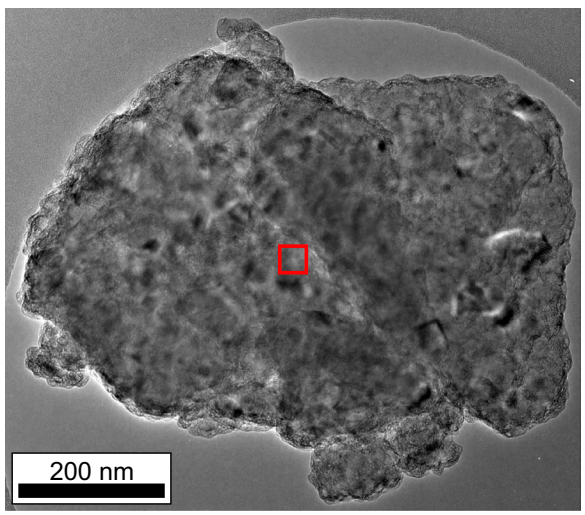

Fig. 1 TEM bright field image of a typical nanocrystalline MgH_2 particle, which is already dehydrogenated due to the impact of the electron beam. The *red square* indicates an area of 36 × 36 nm^2 of the particle, from where the VEEL spectra are acquired with the CCD camera

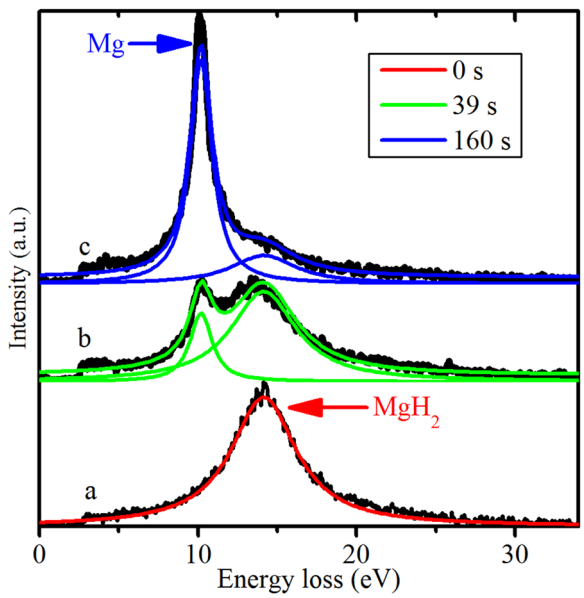

Fig. 2 Three of a series of 106 VEEL spectra acquired from a MgH_2 particle. **a** At the beginning of the electron beam exposure, **b** After 39 s, and **c** after 160 s of continious irradiation. The MgH_2 plasmon at 14.1 eV decreases, while the Mg plasmon at 10.1 eV arises. After roughly 3 min, all hydrogen has left the specimen. The fitted Lorentz functions describing the respective plasmon contributions are overlaid on the experimental data. The adjusted coefficients of determination, $\bar{R}^2$, describing the goodness of the fits are 0.99, 0.97 and 0.98 in **a**–**c**, respectively. The used current density is 818 $e^-/nm^2/s$ at an accelerating voltage of 300 kV

is mostly due to some intensity in between the plasmon peaks, because the MgH_2 plasmon not only decreases in intensity but also shifts to lower energies. The reason for this is the reduction of the density of valence electrons upon dehydrogenation, which leads to the reduced plasmon energy. This shift in plasmon energy cannot be properly accounted for by the fitting procedure, because the fit does not always converge, if also the plasmon energies are fitted. Therefore, they are fixed at the cost of slightly worse fit qualities. The resulting Lorentz functions are overlaid for both plasmons on the experimental data in Fig. 2.

For all spectra of the series the fitted areas of the Lorentz function corresponding to the MgH_2 plasmon are normalized to their initial value and plotted as function of time in Fig. 3. The monotonic decay can be very precisely described by an exponential function $\exp -t/\tau_e$, where t is the time and $\tau_e = 108\,\mathrm{s}$ is the so-called characteristic time, after which only $1/e = 37\,\%$ of the initial material is left. By multiplying τ_e with the current density j, the characteristic electron dose $D_e = \tau_e j = 8.8 \cdot 10^4\ \mathrm{e}^-/\mathrm{nm}^2$ can be determined.

This evaluation is carried out for 14 likewise conducted experiments of electron-beam-induced dehydrogenations at different accelerating voltages (80 and 300 kV). The resulting fit values for the plasmon energies and widths are in the range of $E_1 = 9.99 - 10.37\,\mathrm{eV}$ and $w_1 = 0.84 - 2.17\,\mathrm{eV}$ for Mg and $E_2 = 13.79 - 14.47\,\mathrm{eV}$ and $w_2 = 4.58 - 6.31\,\mathrm{eV}$ for MgH_2. For each investigated MgH_2 particle its relative thickness d/λ at the area, from which the VEEL spectra are acquired, is determined from these spectra. Due to the large number of spectra for each particle this quantity can be calculated with a small uncertainty. All likewise deduced characteristic electron doses are plotted as function of the relative thickness in Fig. 4 as solid symbols. It is apperent from this figure that the characteristic doses measured at 300 kV are generally higher than those measured at 80 kV. Furthermore, there is a clear tendency for the characteristic dose to increase with the relative thickness of the particle, though some measured values deviate from this trend.

Discussion

MgH_2 is unstable in the high vacuum of a TEM (ca. 10^{-8} mbar) at room temperature. The equilibrium pressure for room temperature can be calculated using the Van't Hoff equation and the standard enthalpy of formation of −75 kJ/mol and is in the order of 10^{-4} mbar. The fact that the hydride phase can be detected in the TEM at all can be explained by high kinetic barriers for the dehydrogenation. This is mainly due to the difficult nucleation of Mg which applies to elevated temperatures [8] and is even more difficult at room temperature. However, the electron beam induces a constant source of nuclei forming homogeneously and statistically distributed throughout the specimen. The diffusion of hydrogen through the particles into vacuum is very fast along the twinning planes, which result from ball milling [8]. Another diffusion path is through the voids [26], that are forming upon dehydrogenation, because of a shrinkage of the material by roughly 25 %. Therefore, hydrogen diffusion away from a growing Mg nucleus cannot limit the dehydrogenation.

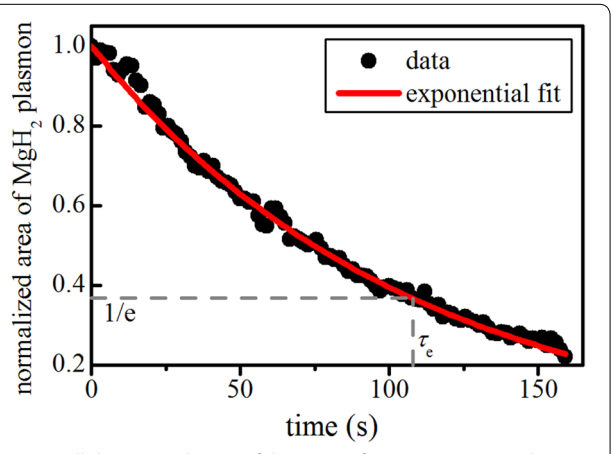

Fig. 3 All determined areas of the Lorenz function corresponding to the MgH_2 plasmon are normalized and plotted as function of time. An exponential decay function is fitted to the normalized areas (*solid red line*)

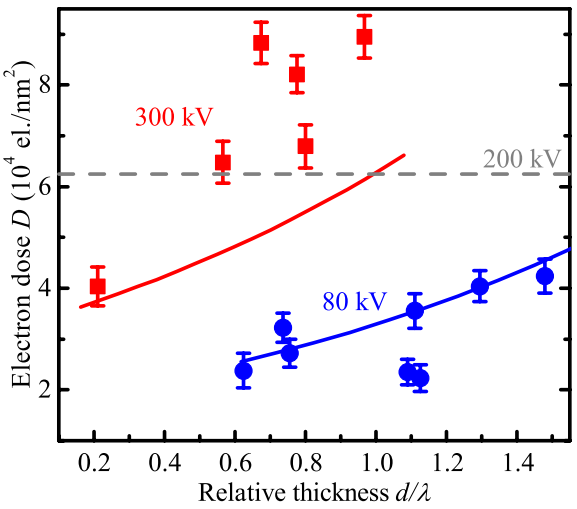

Fig. 4 Deduced electron doses for accelerating voltages of 80 kV (*blue*) and 300 kV (*red*). The characteristic dose determined from the electron diffraction data published by Danaie et al. [22] at 200 kV is shown as the dashed gray horizontal line. The solid lines are calculated characteristic doses assuming single inelastic scattering and a protection factor of 4

However, without the impact of the electron beam we do not observe a further decrease of the amount of the hydride. As soon as the electron beam is switched off the dehydrogenation stops. This is illustrated in Fig. 5, where the temporal evolution of a dehydrogenation is shown, which was interrupted twice for 55 and 68 s by blanking the electron beam. After removing these dark times, the corrected course of the data points follows again a single exponential decay. This clearly shows that spontaneous dehydrogenation does not occur. Since, under the conditions in the TEM, MgH_2 is not the thermodynamic equilibrium phase, this immediately confirms the metastability of the hydride phase and the kinetic impediment of a relaxation into the metallic Mg ground state. The origin of the kinetic barrier involved, however, cannot be identified from the present experiments. It can only be assumed from the fact that the electron beam induced dehydrogenation goes along with the excitation of plasmons that by virtue of the electrical field of the incident electron the metastable hydride becomes locally unstable

The characteristic electron doses shown in Fig. 4 are compared with the value that was determined from electron diffraction data published by Danaie et al. for a comparable dehydrogenation experiment on ball milled MgH_2 at an accelerating voltage of 200 kV [22]. For this, the relative thickness is unknown, but the characteristic electron dose is in good agreement with our results and fits in the range of doses measured for 80 and 300 kV.

The question of the mechanism of the electron beam damage could be answered by first considering beam heating. According to Egerton and Malac [27], however, the expected temperature increase for a typical TEM experiment is only 1 K or even less. Since the beam current for the here discussed dehydrogenation experiments is uncommonly small, no significant beam heating can be expected. Another well-known damage mechanism is atomic displacement or knock-on damage, which can also lead to sputtering. Here, the electron beam damage is generally larger for higher incident electron energies [27]. This, however, is in clear contrast to our experimental observations, where the characteristic electron doses are higher at 300 keV than at 80 keV, i.e. the hydride can withstand a higher dose and there is less damage at 300 keV. This result rather clearly indicates that the dominating electron beam damage to the hydride is radiolysis [20], because it scales with the scattering cross section, which is higher for 80 keV electrons [27]. Here, the high-energy electrons disturb the ionic metal–hydrogen bond. Since MgH_2 is unstable in vacuum, all released hydrogen desorbs instantaneously from the specimen.

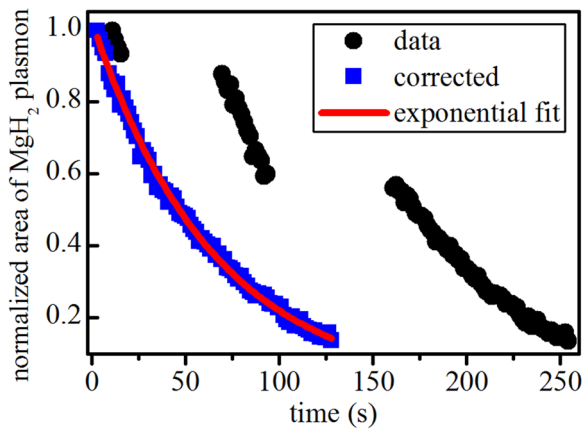

Fig. 5 The normalized areas of the MgH_2 plasmon are plotted as function of time for a dehydrogenation, which was paused twice by blanking the electron beam. The original data (*black dots*) is corrected for the interruptions (*blue squares*) and then follows a single exponential decay (*red line*)

For the dehydrogenation of MgH_2, some energy transfer is needed to overcome the kinetic barrier given by the activation energy of 127 kJ mol^{-1} for dehydrogenation [8]. In units of electronvolts this converts to 1.3 eV per MgH_2 molecule. This means that in principle every inelastically scattering electron, which excites a MgH_2 plasmon, can cause the dehydrogenation of a MgH_2 molecule. It is well possible that the cross sections for radiolysis and the inelastic scattering are equal, i.e. $\sigma_{rad} = \sigma_{in} = \sigma$. To validate this assumption we first calculate the energy-differential cross section for the inelastic scattering of an incident high-energy electron by a plasmon up to an angle β. It is given by [28]:

$$\frac{d\sigma(\beta)}{dE} \approx \frac{1}{\pi a_0 m_0 v^2 n_a} \frac{EwE_p^2}{(E^2 - E_p^2)^2 + (Ew)^2} \ln(1 + \beta^2/\theta_E^2)$$
$$\text{with } n_a = \frac{3\rho N_A}{M} \quad \text{and } \theta_E = \frac{E}{\gamma m_0 v^2}, \tag{3}$$

where a_0 is the Bohr radius, m_0 is the electron rest mass, v is the relativistic electron velocity, n_a represents the volume density of the atoms in the medium given by the mass density $\rho = 1.45\ g/cm^3$ and the molecular mass $M = 26.3\ g/mol$ of MgH_2 (N_A is the Avogadro constant), and $\gamma^2 = \left(1 - v^2/c^2\right)^{-1}$ is the Lorentz factor. Here, γ and v depend on the incident electron energy E_0. $E_p = 14\,eV$ and $w = 5\,eV$ are the plasmon energy and width of the MgH_2 plasmon peak, respectively. Equation (3) is only valid for scattering up to angles β smaller than the plasmon cutoff angle θ_c of typically 10 mrad. In practice, plasmon excitations can cause inelastic scattering to angles larger than this cutoff angle. Hence, the total inelastic scattering cross section σ is typically up to 20 % larger [28]. This cross section can be obtained by integrating Eq. (3) over the energy loss E. We use the software package

Mathematica for the numerical integration up to an energy loss of 50 eV and for incident electron energies of 80 and 300 keV. According to Poisson statistics, the probability for n-fold inelastic scattering is [24]

$$P_n = (1/n!)(d/\lambda)^n \exp(-d/\lambda), \quad (4)$$

where d is the thickness of the specimen and λ is the mean free path for inelastic scattering. Each scattering event causes the breaking of a Mg–H bond. Therefore, the rate of dehydrogenation, i.e. the change of the number of Mg–H bonds as function of time is given by

$$\frac{dN(t)}{dt} = -\sum_{n=0}^{\infty} nP_n I, \quad (5)$$

where N is the number of Mg–H bonds at time t and I is the electron beam current. It can be shown that this expression simplifies to (see "Appendix" section)

$$\frac{dN(t)}{dt} = -3/2N\sigma j. \quad (6)$$

Here, j is the current density. Integration of Eq. (6) leads to

$$N(t) = N_0 \exp\left(-j\sigma t\right), \quad (7)$$

where N_0 is the initial amount of Mg–H bonds. This relation does describe the experimentally observed decay of the MgH_2 plasmon, but it cannot explain the observed thickness dependence of the characteristic electron dose as shown in Fig. 4: Thinner particles show smaller characteristic electron doses, i.e. they dehydrogenate faster than thicker particles.

Equation 7 does not describe the experimentally determined thickness dependence, because Eq. (5) is valid for thick specimens, where multiple inelastic scattering can take place. In contrast the studied MgH_2 particles are relatively thin so that predominantly single scattering occurs. An example VEEL spectrum of a relatively thick particle with $d/\lambda = 1.5$ is displayed in Additional file 2: Figure S2. Mainly the single loss plasmon peak is present and only a small contribution from plural scattering at higher energies can be observed, which confirms that mainly single scattering occurs. Therefore, the sum in Eq. (5) is terminated at $n = 1$ and $N(t)$ is given by the differential equation

$$\begin{aligned}\frac{dN(t)}{dt} &= -d/\lambda \exp(-d/\lambda)I \\ &= -3/2dN(t)/V\sigma \exp(-3/2dN(t)/V\sigma)jA, \quad (8)\end{aligned}$$

where the mean free path is written using $N(t)$ as $1/\lambda = n_a\sigma = 3/2N(t)/V\sigma$ (see "Appendix" section). The particle morphology is approximated by a sphere of diameter d with the volume V and the projected area A. Using the initial condition $N(t = 0) = N_0 = 2\rho N_A/MV$ the differential Eq. (8) can be solved numerically and the characteristic time τ_e, for which $N(\tau_e) = N_0/e$, can be determined. In this way we calculate the characteristic electron doses $D_e = \tau_e j$ for different thicknesses at electron energies of 80 and 300 keV using the software package Mathematica. In Fig. 4 the calculated electron doses are compared with the experimental data. There is a good qualitative agreement between both; however, they differ by a factor of roughly 4. The good agreement between experiment and theory suggests (although it does not prove) that one plasmonic excitation per molecule is responsible for the radiolytic damage, i.e. the cross sections for radiolysis and inelastic scattering by a plasmon are indeed the same [27]. But based on the inelastic scattering, the effective electron dose should be four times smaller than our experimental results, meaning that the hydride should be even more sensitive to the electron beam. This discrepancy can be explained by the presence of a thin nanocrystalline or amorphous MgO and $Mg(OH)_x$ surface layer (3–4 nm) surrounding the MgH_2 particles, whose formation cannot be completely avoided. Despite the usage of the vacuum transfer holder, such a thin oxide layer may have already formed during sample handling under argon inside the glove box [29]. This oxide layer acts as a diffusion barrier for the hydrogen and, therefore, slows down the dehydrogenation. Such a protective effect is also known from carbon or metal coatings for organic or low Z materials, where protection factors of up to 6 are reported [27]. Therefore, the calculated characteristic electron doses displayed in Fig. 4 are multiplied by this protection factor of 4. As a consequence, the values also agree quantitatively very well at 80 keV. For 300 keV, the data scattering is stronger. This may be due to drift or rotation of the particles during the dehydrogenation, which would mean that during the measurement, the region of the particle for the acquisition of the VEEL spectra may change. This could result in an inaccurate thickness measurement and an erroneous measurement of the actual current density due to an inhomogeneous illumination. Furthermore, the experimental electron doses are still larger than the theoretical values which are corrected by the protection factor and an even larger factor would have to be assumed, which does not make sense, because the diffusion of hydrogen through the oxide layer should not depend on the electron energy. Another possible interpretation, however, is that the cross sections for inelastic scattering and radiolysis are not equal and the difference further depends on the electron energy. In both cases, we can show with the here developed methodology that the cross sections have at least the same order of magnitude and that mainly single scattering takes place, which explains the thickness dependence of the characteristic electron doses.

Danaie et al. observed strong evidence of the core-shell morphology for the electron-beam-induced dehydrogenation of MgH_2 at room temperature using EFTEM [8]. Metallic Mg started to grow at the surface and forms a shell around the shrinking hydride core. This observation can be well explained by the theory based on single scattering as described above. The particles studied by Danaie et al. show sizes comparable to the particles studied by us, because the VEEL spectrum published in that reference [8] also shows just a minor plural scattering contribution and the published EFTEM images also reveal a cross section of the particles of roughly 200–400 nm. At the shell, where the particle is thinner (in the direction of the electron beam), the dehydrogenation happens faster than in the thicker core, where too many Mg–H bonds are present to be dehydrogenated with the same rate as in the thinner regions just by single scattering. This again shows that the diffusion of hydrogen does not play a role for this process and does not limit the speed of the dehydrogenation.

The measured characteristic electron doses for the dehydrogenation of MgH_2 are in the order of 10^4 e^-/nm^2. For a typical TEM investigation, the electron dose is at least two orders of magnitude larger, especially for analytical and high-resolution studies. Hence, these types of analyses can only be conducted for the dehydrogenated state and not the hydride phase. This is in particular problematic for very thin and nanostructured specimens. And this problem is not only relevant for MgH_2, but applies also to other hydrides such as $LiBH_4$ [30], AlH_3 [31], $LiAlH_4$, $NaBH_4$ [32], $NaAlH_4$ [33] or LiH [34]. The major drawback is that upon dehydrogenation the specimen undergoes significant structural and morhpological changes that may also include phase separations, and any information gathered for the dehydrogenated state cannot be applied to the original hydride phase. A solution might be the cryogenic cooling of the specimen, because at 77 K the equilibrium pressure of MgH_2 is reduced to 10^{-41} mbar, which is well below the hydrogen partial pressure of 10^{-10} mbar in the TEM. As a consequence, the hydride should be stable under these conditions. However, also in cryo TEM studies, the radiolytic decomposition of MgH_2 has been reported, although on a longer time scale of up to 15 min [8]. Another possibility might be the usage of coatings with thicknesses of tens of nm, that on the one hand would lead to higher protection factors, but on the other hand would alter the properties of the specimen and reduce the TEM image contrast. A more promising approach is performing the TEM analysis at an elevated hydrogen back pressure rather than vacuum to stabilize the hydride phase. Hydrogen pressures of up to 4.5 bar can be realized with recently developed closed environmental cell TEM holders for in-situ experiments, as they have already been used for studying the (de)hydrogenation of nanostructured Pd [35].

Conclusions

In this study we present a detailed and quantitative analysis of the electron-beam-induced dehydrogenation of nanocrystalline MgH_2. We use VEELS to investigate this phenomenon in-situ in a monochromated TEM under low-dose conditions. MgH_2 is metastable in high vacuum and only kinetically stabilized, because the nucleation of Mg is difficult, especially at room temperature. The electron beam, however, generates nucleation sites for the Mg phase throughout the particle, but the metal phase does not grow by itself at the accessible time scale of minutes due to slow reaction kinetics. Hence, the observed dehydrogenation is solely induced by the electron illumination. Based on the derived characteristic electron doses for acceleration voltages of 80 kV and 300 kV, we show that the radiolytic decomposition is caused by the inelastic scattering of the incident electrons. The rate of the dehydrogenation increases with increasing electron current density and decreasing specimen thickness. A discrepancy between the experimental doses and from the inelastic scattering cross section calculated doses by a factor of roughly 4 points to a kinetic barrier for the dehydrogenation due to the thin native surface oxide layer. The sensitivity of the MgH_2 to the electron beam is so high that a high-resolution TEM study of unprotected nanostructured MgH_2 with large electron doses is not feasible. The obtained insights of this study are also applicable to other hydrides, which are relevant for solid-state hydrogen storage. The results of this study will help to perform and correctly interpret TEM investigations of such nanostructured hydrides in future.

Additional files

Additional file 1: Figure S1. X-ray diffraction pattern of ball milled MgH_2 and the corresponding Rietveld refinement.

Additional file 2: Figure S2. VEEL spectrum of a MgH_2 particle with a relative thickness of $d/\lambda = 1.5$ at 80 kV. The raw data as well as the deconvoluted spectrum are plotted.

Authors' contributions

AS conducted the TEM experiments, analyzed the results and wrote the manuscript. BR contributed to the discussion and to writing the manuscript. LS supervised the work and reviewed the manuscript. All authors read and approved the final manuscript.

Author details

[1] IFW Dresden, Institute for Metallic Materials, 01171, 270116 Dresden, Germany. [2] TU Dresden, Institut für Festkörperphysik, 01062 Dresden, Germany.

Acknowledgements

The work of A.S. is supported by the Reimer Lemoine Foundation and the TU Dresden Graduate Academy. We are grateful to I. Lindemann, C. Bonatto Minella, and E. Hadjixenophontos for helpful discussions and to M. Herrich and B. Gebel for their technical assistance.

Competing interests
The authors declare that they have no competing interests.

Appendix

In order to derive Eq. (6), we first show that $\sum_{n=0}^{\infty} nP_n = d/\lambda$: I.e., it is to be shown that

$$\lambda/d \sum_{n=1}^{\infty} nP_n = 1$$

With Eq. (4) this becomes

$$\lambda/d \sum_{n=1}^{\infty} nP_n = \lambda/d \left\{ 0 \cdot P_0 + \sum_{n=1}^{\infty} n(1/n!)(d/\lambda)^n \exp(-d/\lambda) \right\}$$
$$= \sum_{n=1}^{\infty} (1/(n-1)!)(d/\lambda)^{n-1} \exp(-d/\lambda),$$

with $m = n - 1$ we can rewrite the summation to

$$= \sum_{m=0}^{\infty} (1/m!)(d/\lambda)^m \exp(-d/\lambda) = \sum_{m=0}^{\infty} P_m = 1, \quad \text{q.e.d.,}$$

because the Poisson distribution is normalized. Inserting this in Eq. (5) yields

$$\frac{dN(t)}{dt} = -d/\lambda I$$

and using $I = jA$ and $1/\lambda = n_a \sigma$ [24] this can be written as

$$\frac{dN(t)}{dt} = -d n_a \sigma j A.$$

The atom density for MgH_2 is given by $n_a = 3\rho N_A/M = 3N_{MgH_2}/V$ [cf. Eq. (3)], where N_{MgH_2} is the number of MgH_2 molecules. Since $N(t)$ describes the number of Mg–H bonds and since each MgH_2 molecule contains two bonds, it follows that $N_{MgH_2} = N(t)/2$. Accordingly, the atom density can be written as $n_a = 3/2N(t)/V$, which yields

$$\frac{dN(t)}{dt} = -3/2 dN(t)/V \sigma j A \quad = -3/2 N(t) \sigma j,$$

because d and A cancel with V.

Received: 1 April 2016 Accepted: 6 June 2016
Published online: 23 June 2016

References

1. Aguey-Zinsou, K.F., Ares-Fernandez, J.R.: Hydrogen in magnesium: new perspectives toward functional stores. Energy Environ. Sci. **3**, 526–543 (2010)
2. Schlapbach, L., Züttel, A.: Hydrogen-storage materials for mobile applications. Nature **414**, 353–358 (2001)
3. Jia, Y., Sun, C., Shen, S., Zou, J., Mao, S.S., Yao, X.: Combination of nanosizing and interfacial effect: Future perspective for designing Mg-based nanomaterials for hydrogen storage. Renew. Sust. Energ. Rev. **44**, 289–303 (2015)
4. Sakintuna, B., Lamari-Darkrim, F., Hirscher, M.: Metal hydride materials for solid hydrogen storage: a review. Int. J. Hydrog. Energy. **32**, 1121–1140 (2007)
5. Huot, J., Liang, G., Boily, S., Van Neste, A., Schulz, R.: Structural study and hydrogen sorption kinetics of ball-milled magnesium hydride. J. Alloys. Compd. **293–295**, 495–500 (1999)
6. Varin, R., Czujko, T., Wronski, Z.: Particle size, grain size and γ-MgH_2 effects on the desorption properties of nanocrystalline commercial magnesium hydride processed by controlled mechanical milling. Nanotechnology **17**, 3856 (2006)
7. Danaie, M., Mitlin, D.: TEM analysis and sorption properties of high-energy milled MgH_2 powders. J. Alloys. Compd. **476**, 590–598 (2009)
8. Danaie, M., Tao, S., Kalisvaart, P., Mitlin, D.: Analysis of deformation twins and the partially dehydrogenated microstructure in nanocrystalline magnesium hydride (MgH_2) powder. Acta. Mater. **58**, 3162–3172 (2010)
9. Wagemans, R.W.P., van Lenthe, J.H., de Jongh, P.E., van Dillen, A.J., de Jong, K.P.: Hydrogen storage in magnesium clusters: quantum chemical study. J. Am. Chem. Soc. **127**, 16675–16680 (2005)
10. Kim, K.C., Dai, B., Johnson, J.K., Sholl, D.S.: Assessing nanoparticle size effects on metal hydride thermodynamics using the Wulff construction. Nanotechnology **20**, 204001 (2009)
11. de Jongh, P.E., Wagemans, R.W.P., Eggenhuisen, T.M., Dauvillier, B.S., Radstake, P.B., Meeldijk, J.D., Geus, J.W., de Jong, K.P.: The preparation of carbon-supported magnesium nanoparticles using melt infiltration. Chem. Mater. **19**, 6052–6057 (2007)
12. Jeon, K.J., Moon, H.R., Ruminski, A.M., Jiang, B., Kisielowski, C., Bardhan, R., Urban, J.J.: Air-stable magnesium nanocomposites provide rapid and high-capacity hydrogen storage without using heavy-metal catalysts. Nat. Mater. **10**, 286–290 (2011)
13. Makridis, S.S., Gkanas, E.I., Panagakos, G., Kikkinides, E.S., Stubos, A.K., Wagener, P., Barcikowski, S.: Polymer-stable magnesium nanocomposites prepared bylaser ablation for efficient hydrogen storage. Int. J. Hydrog. Energy **38**, 11530–11535 (2013)
14. Zhang, S., Gross, A.F., Van Atta, S.L., Lopez, M., Liu, P., Ahn, C.C., Vajo, J.J., Jensen, C.M.: The synthesis and hydrogen storage properties of a MgH_2 incorporated carbon aerogel scaffold. Nanotechnology **20**, 204027 (2009)
15. Mooij, L.P., Baldi, A., Boelsma, C., Shen, K., Wagemaker, M., Pivak, Y., Schreuders, H., Griessen, R., Dam, B.: Interface energy controlled thermodynamics of nanoscale metal hydrides. Adv. Energy. Mater. **1**, 754–758 (2011)
16. Kalidindi, S.B., Jagirdar, B.R.: Highly monodisperse colloidal magnesium nanoparticles by room temperature digestive ripening. Inorg. Chem. **48**, 4524–4529 (2009)
17. Aguey-Zinsou, K.F., Ares-Fernndez, J.R.: Synthesis of colloidal magnesium: a near room temperature store for hydrogen. Chem. Mater. **20**, 376–378 (2008)
18. Anastasopol, A., Pfeiffer, T.V., Middelkoop, J., Lafont, U., Canales-Perez, R.J., Schmidt-Ott, A., Mulder, F.M., Eijt, S.W.H.: Reduced enthalpy of metal hydride formation for Mg-Ti nanocomposites produced by spark discharge generation. J. Am. Chem. Soc. **135**, 7891–7900 (2013)
19. Jia, Y., Sun, C., Cheng, L., Wahab, M.A., Cui, J., Zou, J., Zhu, M., Yao, X.: Destabilization of Mg-H bonding through nano-interfacial confinement by unsaturated carbon for hydrogen desorption from MgH_2. Phys. Chem. Chem. Phys. **15**, 5814 (2013)
20. Schober, T., Chason, M.K.: A CTEM AND HVEM STUDY OF HYDRIDE PRECIPITATION IN MAGNESIUM. Metal-Hydrogen Systems, pp. 177–184. Pergamon, Oxford (1982)
21. Paik, B., Jones, I., Walton, A., Mann, V., Book, D., Harris, I.: $MgH_2 \rightarrow Mg$ phase transformation driven by a high-energy electron beam: An in situ transmission electron microscopy study. Philos. Mag. Lett. **90**, 1–7 (2010)
22. Danaie, M., Malac, M., Mitlin, D.: Investigation of beam damage mechanism of ball-milled MgH_2 powder. Microsc. Microanal. **14**, 278–279 (2008)
23. Zaluzec, N. J., Schober, T., Westlake D. G.: *Application of EELS to the study of metal-hydrogen systems*. Thirty-ninth annual EMSA meeting, 1981

24. Egerton, R.F.: Electron energy-loss spectroscopy in the electron microscope, 2nd edn. Plenum Press, New York (1989)
25. Lutterotti, L.: Total pattern fitting for the combined size-strain-stress-texture determination in thin film diffraction. Nucl. Instrum. Meth. B **268**, 334–340 (2010)
26. Mooij, L., Dam, B.: Nucleation and growth mechanisms of nano magnesium hydride from the hydrogen sorption kinetics. Phys. Chem. Chem. Phys. **15**, 11501 (2013)
27. Egerton, R.F., Li, P., Malac, M.: Radiation damage in the TEM and SEM. Micron. **35**, 399–409 (2004)
28. Egerton, R. F.: *Electron energy-loss spectroscopy in the electron microscope*. 3rd edn, Springer New York (2011)
29. Friedrichs, O., Snáchez-López, J., López-Cartes, C., Dornheim, M., Klassen, T., Bormann, R., Fernández, A.: Chemical and microstructural study of the oxygen passivation behaviour of nanocrystalline Mg and MgH_2. Appl. Surf. Sci. **252**, 2334–2345 (2006)
30. House, S.D., Liu, X., Rockett, A.A., Majzoub, E.H., Robertson, I.M.: Characterization of the dehydrogenation process of $LiBH_4$ confined in nanoporous carbon. J. Phys. Chem. C. **118**, 8843–8851 (2014)
31. Ikeda, K., Muto, S., Tatsumi, K., Menjo, M., Kato, S., Bielmann, M., Züttel, A., Jensen, C.M., Orimo, S.: Dehydriding reaction of AlH_3: insitu microscopic observations combined with thermal and surface analyses. Nanotechnology **20**, 204004 (2009)
32. Herley, P.J., Jones, W.: Transmission electron microscopy of beam-sensitive metal hydrides*. Z. Phys. Chem. **147**, 147–159 (1986)
33. Egerton, R.F., Crozier, P.A., Rice, P.: Electron energy-loss spectroscopy and chemical change. Ultramicroscopy. **23**, 305–312 (1987)
34. Deprez, E., Justo, A., Rojas, T.C., López-Cartés, C., Bonatto, C., Minella, C.B., Bösenberg, U., Dornheim, M., Bormann, R., Fernández, A.: Microstructural study of the $LiBH_4$-MgH_2 reactive hydride composite with and without Ti-isopropoxide additive. Acta. Mater. **58**, 5683–5694 (2010)
35. Yokosawa, T., Alan, T., Pandraud, G., Dam, B., Zandbergen, H.: In-situ TEM on (de)hydrogenation of Pd at 0.5-4.5bar hydrogen pressure and 20–400 °C. Ultramicroscopy **112**, 47–52 (2012)